High-Performance Blue-Excitable Yellow Phosphor Obtained from an Activated Solvochromic Bismuth-Fluorophore Metal-Organic Framework

*Benjamin J. Deibert,[†,ϕ] Ever Velasco,[†,ϕ] Wei Liu,[†] Simon J. Teat,[§] William P. Lustig,[†] Jing Li[†,]**

†Department of Chemistry and Chemical Biology, Rutgers, The State University of New Jersey, Piscataway, New Jersey 08854, United States

§Advanced Light Source, Lawrence Berkeley National Laboratory, Berkeley, California 94720, United States.

KEYWORDS: bismuth, chromophore, luminescent MOF, phosphor, White LED

ABSTRACT: We report the synthesis, structure, and photoluminescence properties of a new bismuth based luminescent metal-organic framework (LMOF). The framework is comprised of a 9-coordinated Bi^{3+} building unit and 4', 4''', 4'''', 4'''''-(ethene-1,1,2,2-tetrayl)tetrakis([1,1'-biphenyl]-4-carboxylic acid) (H_4tcbpe) organic linker, which has strong yellow aggregation induced emission (AIE). The structure can be viewed as two interpenetrated 4,4-anionic nets that are stabilized by K^+ ions forming 1-D helical inorganic chains by connecting bismuth nodes through shared oxygen bonds. The as-made LMOF has a bluish emission centered at 459 nm with an internal quantum yield of 57% when excited at 360 nm. The emission properties of the

LMOF were found to be highly solvochromic with respect to DMF. Upon partial solvent removal, the framework undergoes significant red-shifting to a greenish emission centered at 500 nm. Complete removal of DMF results in additional red-shifting fluorescence coupled with structural changes. The resulting material has strong blue-excitable (455 nm) yellow emission centered at 553 nm, with a quantum yield of 74%, which maintains after heating in air for five days at 90 °C. This is the second highest QY value for blue-excited yellow emission among all reported LMOFs.

Luminescent metal-organic frameworks (LMOFs) are currently being studied for use in multiple luminescence-based applications, including chemical sensing, biosensing and biomedical imaging, thermometry, and general lighting.[1-9] Our recent work has established that LMOFs with strong yellow emission are potentially suitable to serve as the yellow phosphor in commercial blue light driven phosphor-converted white light-emitting diodes (PC-WLEDs),[10,11] which are rapidly replacing traditional lighting technologies (incandescent, compact fluorescent), thanks to their lower energy consumption and longer lifetime.[12] A common type of PC-WLEDs utilizes a blue LED to excite a yellow phosphor, such as yttrium aluminum garnet doped with cerium (YAG:Ce^{3+}), resulting in white light through the combination of the blue and yellow emissions.[13,14] Most commercial yellow phosphors are based on rare-earth elements (REE), which are of limited supply yet rising demand, owing to their importance in numerous applications.[15] It is anticipated that over time both their demand and price will continue to rise. Thus, the development of alternative yellow phosphors that are free of REEs is highly desirable.[16]

One approach to designing strongly emissive LMOFs is to integrate a strong organic fluorophore with desired optical properties along with a complementary metal. Previous work reveals that structures based on the tetraphenylethylene core, which has minimal fluorescence in solution but undergoes aggregation induced emission (AIE), show strong photoemission in the blue-yellow range when bound to a framework.[10,11,17-21] Further, our studies have shown that the 4', 4''', 4'''', 4''''''- (ethene-1,1,2,2-tetrayl) tetrakis(([1,1'-biphenyl]-4-carboxylic acid)) (H_4tcbpe) derivative has strong blue-excitable yellow emission (~550 nm), and has proven a prime candidate to construct blue-excitable yellow phosphors.[11] LMOFs constructed with tcbpe show higher internal quantum yields (QY) and improved chemical and thermal stability compared to the ligand.

Bismuth-based materials have previously gained attention for potential use in photoluminescence (PL) related fields.[22-25] Currently, Bi has few commercial applications; it is used mainly in pharmaceuticals and as metallurgical additives. Bismuth is the only non-toxic heavy metal, and is most commonly obtained as a byproduct during Pb, Cu, W, and Sn ore refining.[26] Despite being the last radioactively stable element on the periodic table, the cost of bismuth is relatively low. According to the 2015 Mineral Commodities Survey by the U.S. Department of the Interior, the average price of Bi from 2010 to 2014 was ~$22/kg, which was about the same as the cost of Ni and about 50% cheaper than Co for the same time period. In comparison, the average costs of 1 kg of Ce_2O_3, Eu_2O_3, and Tb_2O_3 were ~$25, $1530, and $1215, respectively.[27]

Bi^{3+} has a stereoactive lone-pair of $6s^2$ electrons, resulting in flexible and often hemidirected coordination geometry.[28,29] Despite rich existing Bi-complex chemistry, and fifteen-plus years of rapid MOF development with thousands of reported structures, there are still only a handful of

reported bismuth based MOFs (we were able to establish < 20).[30-44] Notably, zur Loye and coworkers have reported a number of Bi coordination polymers and their fluorescence properties using pyridine dicarboxylate as ligand.[44-48] Stock, Cheetham and co-workers have also reported a small variety of interesting Bi-MOFs.[32-34,38,39] We ascribe the scarcity of reported Bi based MOFs to a few factors: 1) flexible coordination geometry of Bi^{3+}, with the lone pair often resulting in hemidirected coordination polyhedra and densely packed 1-D and 2-D coordination polymers, 2) tendency of Bi^{3+} to form anionic frameworks as Bi has up to ten coordination sites, 3) hydrolysis reactivity of Bi^{3+} to form oxides and hydroxides, and 4) limited solubility of Bi^{3+} salts.

With these factors considered, we sought to optimize reaction conditions towards growing Bi-MOFs integrating the H_4tcbpe linker. By employing the large tetracarboxylate linker, void space between Bi^{3+} nodes is maximized allowing for more flexible ligand positioning and promoting the formation of 3-D structures. Potassium salt added during synthesis provides +1 charge balancing cations in the event of anionic framework formation. To slow both hydrolysis of the Bi^{3+} cation and MOF crystal growth, we use a significant excess of a competing carboxylate species (modulator). The utilization of mono-carboxylate species, such as benzoic acid and acetic acid, has proven a critical method for obtaining single crystals in MOF synthesis; this has proven especially effective in the case of zirconium based MOFs.[49] Finally we use a bismuth cluster as the metal source in place of commonly utilized $Bi(NO_3)_3 \cdot 5H_2O$ to address solubility and hydrolysis concerns. Utilizing this synthetic strategy, a new BiK-tcbpe LMOF was obtained and its optical properties were studied.

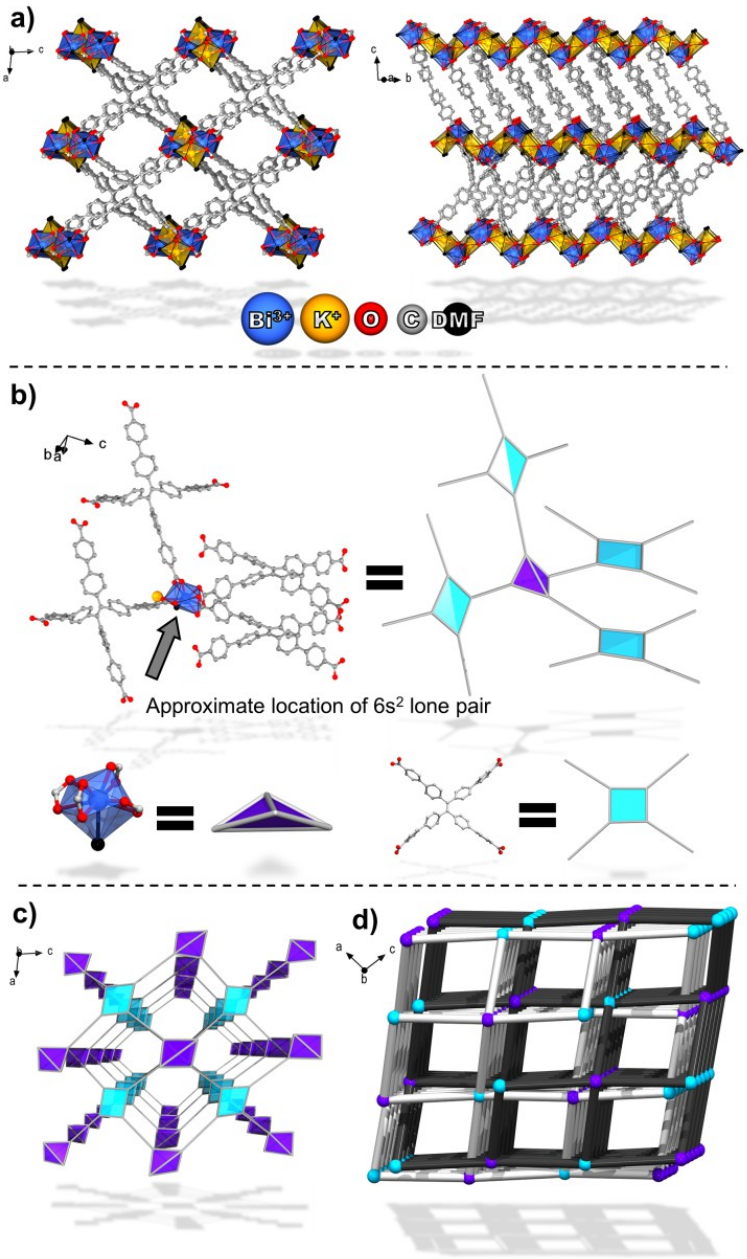

Figure 1. a) Structure plots of 1 along the crystallographic b-axis (left) and slightly rotated from the a-axis (right). b) Coordination geometry of Bi^{3+} with approximate location of $6s^2$ lone pair and polyhedral representation. c) Single Bi-tcbpe 4,4-connected net along the b-axis. d) Line connectivity drawing showing the two-fold interpenetration of the Bi-tcbpe nets.

Single crystals of K[Bi(tcbpe)$(DMF)_2$]·*x*DMF (**1** or **LMOF-401**, Figure 1a, DMF = dimethylformamide), were obtained solvothermally in DMF (100 ˚C, 3 days) with excess benzoic acid added as a synthetic modulating agent (see Supporting Information S2 for synthetic details). An easily prepared Bi-salycilate cluster was selected as the metal source, owing to its ease of preparation, air stability, and solubility in DMF.[50] Reactions using $Bi(NO_3)_2$ or $BiPh_3$ as the metal source in place of the cluster resulted in mixed phases and different products, respectively. **1** crystallizes in a monoclinic crystal system with a C2/c space group (see S3, Table S1); the asymmetric unit has one K^+, Bi^{+3}, tcbpe and two DMF molecules.[51] The Bi^{3+} building unit is overall coordinated to nine oxygen atoms with hemidirectional coordination geometry owing to bismuth's lone pair (Figure 1b). Four carboxylates from four tcbpe linkers form bidentate coordination bonds to Bi^{3+}, with the last oxygen from coordinated DMF. The overall structure can be described as two interpenetrated 4,4-connected anionic 3-D nets comprised of distorted tetrahedral Bi^{3+} and rectangular tcbpe building units (Figures 1b, 1c and 1d). The Bi^{3+} building unit has highly distorted hemidirected tetrahedral geometry with respect to linker connectivity (Figure 1b). Two planes are formed by two each of the four linkers which extend throughout each net. The large linker size promotes some degree of linker flexibility, as observed by a slight warping of each rectangular tcbpe ligand. Potassium cations residing between Bi^{3+} building units form helical 1-D chains that connect and charge balance the two anionic nets through shared μ_3-O carboxylates and coordinated DMF, shown in Figure 1a as the yellow polyhedrons (see Figures S1 and S2 for additional structural depictions).

The observed Bi-carboxylate bonding features align with those reported previously for hemidirected Bi coordination polyhedrons.[34,38,39,44] Each carboxylate pair has one short and one long Bi-O bond, and one of the four carboxylates has slightly longer distances in both cases. The

three short Bi-O carboxylate bond distances are 2.245, 2,283 and 2.336 Å, with corresponding longer Bi-O bonds at 2.619, 2.641, and 2.657 Å, respectively. The last carboxylate has longer distances of 2.480 and 2.705 Å. The coordinated DMF is responsible for longest Bi-O bond (2.884 Å) resulting in gyroenlongation of the Bi^{3+} polyhedron, and shares a μ_3-O bond with K^+ (2.663 Å). Potassium coordinates to the other structural DMF molecule through a lone coordination bond (2.639 Å). The rest of the coordination sphere around K^+ is comprised of shared oxygen atoms from the longest five Bi-O carboxylate bonds. The shortest of these K-O interactions (2.600 Å) corresponds to the longest Bi-O carboxylate, with the rest of the bond distances falling between 2.719 and 2.950 Å. Through these shared carboxylate and DMF oxygen atoms, a 1-D helical chain is formed connecting the two interpenetrated Bi-tcbpe frameworks.

Significant changes in the materials' optical absorption and emission properties were observed after desolvation of the framework, resulting in a highly emissive blue-excitable yellow phosphor when fully "activated" (Figure 2a). This transformation was studied by incrementally desolvating **1** under controlled conditions. The results show evidence of strong solvochromism with respect to DMF content, and irreversible structural and optical changes upon full activation, which likely corresponds to removal of coordinated DMF.

As-made crystals of **1** (Figure 2a, left) are near colorless and have an approximate optical band-gap of 2.70 eV, as estimated from the optical absorption spectrum (Figure S7). Photoexcitation at 360 nm results in strong blueish PL emission with a peak maximum of 459 nm (Figure 2b, black curve, see Figure S8 for excitation spectrum) and an internal QY of 57.7% (±0.3%, see Table S1). The thermogravimetric (TG) data for as-made **1** shows 26.7% weight loss corresponding to ~5.3 calculated DMF molecules per formula unit (Figure S3**)**. The TG profile

has stepwise weight-loss up to ~160 °C, which includes both guest and coordinated DMF molecules. As the structure was desolvated incrementally through both ambient exposure and heating under nitrogen flow, changes in solvent content, optical absorption and emission, and structure were monitored (see S5 of the SI for full details). Figure 2b shows the PL emission of **1** at various stages of solvent removal, and corresponding CIE (Commission International de I'Eclairage) coordinate plots are shown in Figure 2c. The colored legend at the bottom of the figure lists the weight of DMF remaining in the sample, which was confirmed by the TG analysis (see TG profile, 50 – 170 ℃, Figure S3) and the calculated average number of corresponding DMF molecules per formula unit. Changes in the PL excitation and optical absorption spectra were also monitored at various stages and are shown in the supporting information (Figures S7 and S8).

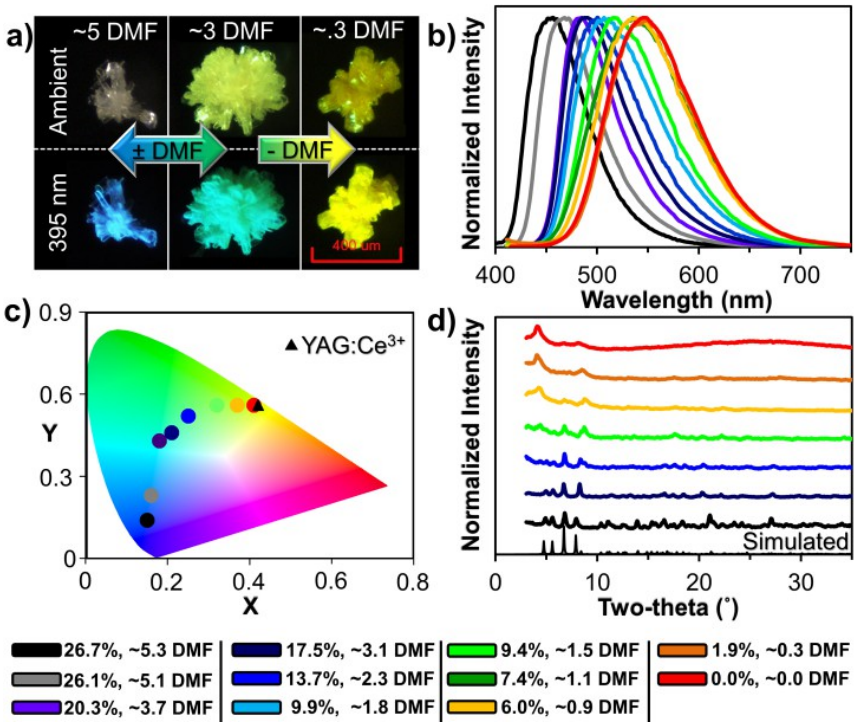

Figure 2. Data for 1 at various stages of desolvation. The colored legend lists the percent weight and estimated number of DMF (per formula unit) remaining in the sample. a) Optical

micrographs under ambient light (top row) and 395 nm UV light (bottom row). b) Emission spectra, λ_{ex} = 360 nm. c) CIE coordinates calculated from the PL spectra. d) PXRD patterns showing structural changes in response to DMF content.

As shown in Figure 2b, as DMF evacuates from **1**, incremental PL red-shifting occurs. When the DMF content reaches below ~3.7 DMF molecules per formula unit (Figure 2, purple), the high-energy side of the PL emission band undergoes minimal displacement compared to the initial red-shift, and instead, band-broadening is observed through red-shifting of the low-energy side of the band. With an average of ~3.1 DMF (Figure 2, navy), **1** appears light-yellow under ambient lighting (Figure 2a, center) and has strong greenish PL emission (λ_{max} = 490 nm), which is still reversible through re-exposure to DMF. The PXRD pattern shows a small lone peak shift from ~8.0˚ to 8.3˚. Below ~2.3 DMF (Figure 2, blue), two new small peaks in the PXRD pattern are observed at ~4.3˚ and 8.7˚ signaling the emergence of a new phase (Figure S5). At this stage, the emission continues to red-shift mainly through band-broadening, but is no longer entirely reversible presumably due to the new phase being formed. The new PXRD peaks at 4.3˚ and 8.7˚ continue to grow in intensity with continued DMF removal, and shift slightly to lower angles. When **1** approaches ~1 DMF, (Figure 2d, gold) the PXRD peaks corresponding to the original phase are a minor contribution to the pattern, which is dominated by the newly formed phase. The PL band-broadening also stops ~1 DMF per unit cell (Figure 2b, dark green, gold), at which point the low energy side of the band remains stationary, but the high energy side begins to red-shift again. This trend continues until the estimated DMF content per unit cell is close to zero, at which point **1** is fully activated and now referred to as **1A**. The PL emission of **1A** (Figure 2b, red trace) has a peak maximum of ~550 nm and is yellow in color (Figure 2c, red circle). The red-shifting trend observed in the PL emission peak of **1** is also observed in the PL excitation and

UV-Vis absorption spectra for various stages of DMF evacuation (Figures S6 and S7). The irreversible structural changes possibly correspond to departure of coordinated DMF molecules, which play an integral role in linking/stabilizing the two anionic nets through K^+. As depicted in Figure S1e, one of the μ_3-O bridges linking potassium to bismuth is from coordinated DMF; loss of this DMF likely results in destabilization if the 1-D inorganic chain resulting irreversible structural changes.

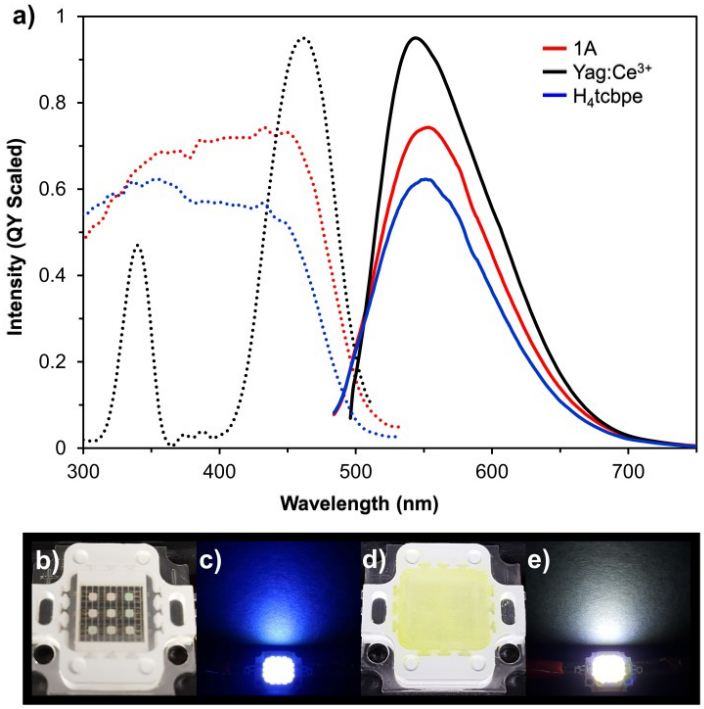

Figure 3. a) QY scaled PL excitation (dotted traces) and emission (λ_{ex} = 455 nm, solid traces) spectra for **1A** (red), YAG:Ce^{3+} (black) and H_4tcbpe (blue); excitation spectra monitored at 553 nm for **1A**, 543 nm for YAG:Ce^{3+}, and 550 nm for H_4tcbpe. b-e) 10W blue LED chip (450-455 nm) uncoated and coated with **1A** under ambient lighting (b,d) and powered on (9V DC) (c, e).

Following full activation by heating at 90 ˚C for five days (Figure 2, red), the excitation spectra for **1A** (monitored at λ_{em} = 553 nm) shows a relative maxima plateau across the blue

region (400 - 455 nm, Figure 3, red dots). The estimated optical bandgap of the activated sample is ~2.3 eV (Figure S6). When excited at 455 nm, **1A** has yellow PL emission (λ_{max} = 553 nm, Figure 3, solid red curve) with CIE coordinates (0.410, 0.560) (Figure 2c), which are comparable to those of YAG:Ce^{3+}; CIE coordinates ≈ (0.420,0.560). The emission maximum of **1A** is slightly red-shifted compared to YAG:Ce^{3+}, however the band is also slightly broader at the base on the high-energy side, resulting in a slightly cooler emission overall. Notably, while not as high as YAG:Ce^{3+} (QY = 95.0%), when compared to reported MOF yellow phosphors, **1A** has the 2nd highest QY of 74.0% (± 0.3%, Tables S2 and S3) when excited by blue light (455 nm). The emission properties of **1A** are similar to that of the pure H_4tcbpe ligand (Figure 3, blue), however with a red-shift in its excitation spectrum, its performance at blue excitation (455 nm) is significantly improved, giving a ~12% increase in QY. The emission profiles for the two are very similar, with **1A** being slightly red-shifted on the high energy side of the emission band. Similarity in their PL profiles suggests that the emission of **1A** is ligand based. A prototype device was fabricated using a 10 W 450-455 nm blue LED to demonstrate the effect of coating with **1A** (Figures 3b - 3e, see SI Section S5 for coating details).

In summary, a new bismuth-potassium-fluorophore LMOF, K[Bi(tcbpe)$(DMF)_2$]·*x*DMF, was obtained using carefully considered synthetic conditions, and it's structural and optical properties were studied. The new material was found to have highly sensitive solvochromic optical properties with respect to guest DMF solvent. The as-made LMOF has strong blue emission with a QY of ~57% that undergoes significant optical red-shifting upon incremental removal of DMF. Upon loss of structurally critical DMF molecules, irreversible structural changes occur paired with additional optical red-shifting. The fully activated material has strong yellow emission (QY

~74%) when excited by 455 nm blue light, making it a promising candidate as an alternative blue-excitable yellow phosphor totally free of REEs.

ASSOCIATED CONTENT

Supporting Information. Chemicals and instrument details, synthetic procedures, single-crystal diffraction results, additional structural drawings, activation procedures and LED coating, TGA, PXRD, UV-Vis, PL and QY data are available in the supporting information. This material is available free of charge via the Internet at http://pubs.acs.org. Crystallographic information is available on the Cambridge Crystallographic Data Center, CCDC #1475408.

AUTHOR INFORMATION

Corresponding Author

*E-mail: Jingli@rutgers.edu; Fax: +1-732-445-5312.

Author Contributions

The manuscript was written through contributions of all authors.

All authors have given approval to the final version of the manuscript.

ϕ These authors contributed equally.

Funding Sources

The RU team would like to acknowledge the support by the National Science Foundation through grant No. DMR-1507210. The Advanced Light Source (ALS) is supported by the

Director, Office of Science, Office of Basic Energy Science, of the U.S. Department of Energy, under contract DE-AC02-05CH11231.

REFERENCES

(1) Allendorf, M. D.; Bauer, C. A.; Bhakta, R. K.; Houk, R. J. T. *Chem. Soc. Rev.* **2009**, *38*, 1330-1352.

(2) Cui, Y.; Yue, Y.; Qian, G.; Chen, B. *Chem. Rev.* **2012**, *112*, 1126-1162.

(3) Hu, Z.; Deibert, B. J.; Li, J. *Chem. Soc. Rev.* **2014**, *43*, 5815-5840.

(4) Deibert, B. J.; Li, J. *Chem. Commun.* **2014**, *50*, 9636-9639.

(5) Lan, A.; Li, K.; Wu, H.; Olson, D. H.; Emge, T. J.; Ki, W.; Hong, M.; Li, J. *Angew. Chem. Int. Ed.* **2009**, *48*, 2334-2338.

(6) Pramanik, S.; Zheng, C.; Zhang, X.; Emge, T. J.; Li, J. *J. Am. Chem. Soc.* **2011**, *133*, 4153-4155.

(7) Azhdari Tehrani, A.; Ghasempour, H.; Morsali, A.; Makhloufi, G.; Janiak, C. *Cryst. Growth Des.* **2015**, *15*, 5543-5547.

(8) He, J.; Zeller, M.; Hunter, A. D.; Xu, Z. *J. Am. Chem. Soc.* **2012**, *134*, 1553-1559.

(9) Kang, Y.; Wang, F.; Zhang, J.; Bu, X. *J. Am. Chem. Soc.* **2012**, *134*, 17881-17884.

(10) Gong, Q.; Hu, Z.; Deibert, B. J.; Emge, T. J.; Teat, S. J.; Banerjee, D.; Mussman, B.; Rudd, N. D.; Li, J. *J. Am. Chem. Soc.* **2014**, *136*, 16724-16727.

(11) Hu, Z.; Huang, G.; Lustig, W. P.; Wang, F.; Wang, H.; Teat, S. J.; Banerjee, D.; Zhang, D.; Li, J. *Chem. Commun.* **2015**, *51*, 3045-3048.

(12) U. S. Department of Energy, *Solid State Lighting. http://energy.gov/eere/ssl/solid-state-lighting.*

(13) Fasol, G.; Nakamura, S. *The Blue Laser Diode, GaN Based Light Emitters and Lasers*; Springer Berlin Heidelberg, 1997.

(14) Xie, R.-J.; Hirosaki, N.; Sakuma, K.; Yamamoto, Y.; Mitomo, M. *Appl. Phys. Lett.* **2004**, *84*, 5404-5406.

(15) Shang, M.; Li, C.; Lin, J. *Chem. Soc. Rev.* **2014**, *43*, 1372-1386.

(16) Bauer, D.; Diamond, D.; Li, J.; McKittrick, M.; Sandalow, D.; Telleen, P. Energy, U. S. Department of Energy, *Critical Materials Strategy*. 2011.

(17) Hu, Z.; Lustig, W. P.; Zhang, J.; Zheng, C.; Wang, H.; Teat, S. J.; Gong, Q.; Rudd, N. D.; Li, J. *J. Am. Chem. Soc.* **2015**, *137*, 16209-16215.

(18) Wei, Z.; Gu, Z.-Y.; Arvapally, R. K.; Chen, Y.-P.; McDougald, R. N.; Ivy, J. F.; Yakovenko, A. A.; Feng, D.; Omary, M. A.; Zhou, H.-C. *J. Am. Chem. Soc.* **2014**, *136*, 8269-8276.

(19) Shustova, N. B.; Cozzolino, A. F.; Reineke, S.; Baldo, M.; Dincă, M. *J. Am. Chem. Soc.* **2013**, *135*, 13326-13329.

(20) Shustova, N. B.; McCarthy, B. D.; Dincă, M. *J. Am. Chem. Soc.* **2011**, *133*, 20126-20129.

(21) Shustova, N. B.; Ong, T.-C.; Cozzolino, A. F.; Michaelis, V. K.; Griffin, R. G.; Dincă, M. *J. Am. Chem. Soc.* **2012**, *134*, 15061-15070.

(22) Datta, R. K. *J. Electrochem. Soc.* **1967**, *114*, 1137-1142.

(23) Dianov, E. M. *Light Sci Appl* **2012**, *1*, e12.

(24) Setlur, A. A.; Srivastava, A. M. *Opt. Mater.* **2006**, *29*, 410-415.

(25) Sun, H.-T.; Sakka, Y.; Shirahata, N.; Matsushita, Y.; Deguchi, K.; Shimizu, T. *J. Phys. Chem. C.* **2013**, *117*, 6399-6408.

(26) Ojebuoboh, F. K. *JOM*, *44*, 46-49.

(27) US Department of the Interior, U.S. Geological Survey; Mineral Commodity Summaries. 2015.

(28) Stavila, V.; Davidovich, R. L.; Gulea, A.; Whitmire, K. H. *Coord. Chem. Rev.* **2006**, *250*, 2782-2810.

(29) Yang, N.; Sun, H. *Coord. Chem. Rev.* **2007**, *251*, 2354-2366.

(30) Busch, S.; Stein, I.; Ruschewitz, U. *Z. Anorg. Allg. Chem.* **2012**, *638*, 2098-2101.

(31) Chen, X.; Cao, Y.; Zhang, H.; Chen, Y.; Chen, X.; Chai, X. *J. Solid State Chem.* **2008**, *181*, 1133-1140.

(32) Feyand, M.; Koppen, M.; Friedrichs, G.; Stock, N. *Chem. Eur. J.* **2013**, *19*, 12537-12546.

(33) Feyand, M.; Mugnaioli, E.; Vermoortele, F.; Bueken, B.; Dieterich, J. M.; Reimer, T.; Kolb, U.; de Vos, D.; Stock, N. *Angew. Chem. Int. Ed. Engl.* **2012**, *51*, 10373-10376.

(34) Inge, A. K.; Koppen, M.; Su, J.; Feyand, M.; Xu, H.; Zou, X.; O'Keeffe, M.; Stock, N. *J. Am. Chem. Soc.* **2016**, *138*, 1970-1976.

(35) Savage, M.; Yang, S.; Suyetin, M.; Bichoutskaia, E.; Lewis, W.; Blake, A. J.; Barnett, S. A.; Schroder, M. *Chem. Eur. J.* **2014**, *20*, 8024-8029.

(36) Shi, F.-N.; Silva, A. R.; Yang, T.-H.; Rocha, J. *CrystEngComm* **2013**, *15*, 3776.

(37) Sun, Y.-Q.; Ge, S.-Z.; Liu, Q.; Zhong, J.-C.; Chen, Y.-P. *CrystEngComm* **2013**, *15*, 10188.

(38) Thirumurugan, A.; Cheetham, A. K. *Eur. J. Inorg. Chem.* **2010**, *2010*, 3823-3828.

(39) Thirumurugan, A.; Tan, J.-C.; Cheetham, A. K. *Cryst. Growth Des.* **2010**, *10*, 1736-1741.

(40) Tran, D. T.; Chu, D.; Oliver, A. G.; Oliver, S. R. J. *Inorg. Chem. Commun.* **2009**, *12*, 1081-1084.

(41) Tröbs, L.; Wilke, M.; Szczerba, W.; Reinholz, U.; Emmerling, F. *CrystEngComm* **2014**, *16*, 5560-5565.

(42) Wang, G.; Liu, Y.; Huang, B.; Qin, X.; Zhang, X.; Dai, Y. *Dalton Trans.* **2015**, *44*, 16238-16241.

(43) Wang, G.; Sun, Q.; Liu, Y.; Huang, B.; Dai, Y.; Zhang, X.; Qin, X. *Chem. Eur. J.* **2015**, *21*, 2364-2367.

(44) Wibowo, A. C.; Smith, M. D.; zur Loye, H.-C. *Cryst. Growth Des.* **2011**, *11*, 4449-4457.

(45) Wibowo, A. C.; Smith, M. D.; Yeon, J.; Halasyamani, P. S.; zur Loye, H.-C. *J. Solid State Chem.* **2012**, *195*, 94-100.

(46) Wibowo, A. C.; Smith, M. D.; zur Loye, H.-C. *CrystEngComm* **2011**, *13*, 426-429.

(47) Wibowo, A. C.; Smith, M. D.; zur Loye, H. C. *Chem. Commun.* **2011**, *47*, 7371-7373.

(48) Wibowo, A. C.; Vaughn, S. A.; Smith, M. D.; Zur Loye, H. C. *Inorg. Chem.* **2010**, *49*, 11001-11008.

(49) Bai, Y.; Dou, Y.; Xie, L.-H.; Rutledge, W.; Li, J.-R.; Zhou, H.-C. *Chem. Soc. Rev.* **2016**.

(50) Boyd, T. D.; Kumar, I.; Wagner, E. E.; Whitmire, K. H. *Chem. Commun.* **2014**, *50*, 3556-3559.

(51) Crystal Data for K[Bi(tcbpe)$(DMF)_2$]·*x*DMF (LMOF-401), $C_{60}H4_6BiKN_2O_{10}$, FW: 1203.07, a = 32.0791(13) Å, b = 11.9048(5) Å, c = 37.7384(15) Å, α = 90°, β = 99.269(2)°, γ = 90°, synchrotron radiation (λ = 0.7749 Å), T = 100 K, monoclinic, C2/c, Z=8, absorption coefficient = 2.793 mm^{-1}, F(000) = 4816, reflections collected = 60475, independent reflections = 13085 [R(int) = 0.0804], final R indices [I>2sigma(I)]: R1 = 0.0465, wR2 = 0.1112, R indices (all data): R1 = 0.0628, wR2 = 0.1168, GoF = 1.023.

For Table of Contents Use Only

High-Performance Blue-Excitable Yellow Phosphor Obtained from an Activated Solvochromic Bismuth-Fluorophore Metal-Organic Framework

Benjamin J. Deibert, Ever Velasco, Wei Liu, Simon J. Teat, William P. Lustig, Jing Li

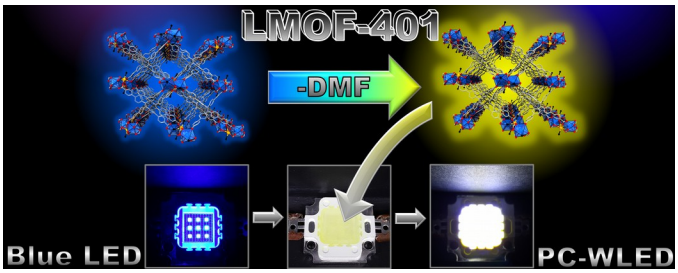

LMOF-401 is a rare example of a Bi-fluorophore LMOF with strong blue emission that converts to green and finally yellow upon removal of DMF molecules within the structure. The fully activated material shows strong yellow emission (~74% QY) under blue light (455 nm) excitation, and demonstrates promise for use as the phosphor coating in phosphor-converted white LEDs (PC-WLEDs).